Tetrahedron 67 (2011) 2025–2034

Contents lists available at ScienceDirect

Tetrahedron

journal homepage: www.elsevier.com/locate/tet

# Hydrazones from hydroxy naphthaldehydes and *N*-aminoheterocycles: structure and stereodynamics

R. Fernando Martínez [a,*], Martín Ávalos [a], Reyes Babiano [a], Pedro Cintas [a], Mark E. Light [b], José L. Jiménez [a], Juan C. Palacios [a], Esther M.S. Pérez [a], Vicenta Rastrojo [a]

[a] Departamento de Química Orgánica e Inorgánica, QUOREX Research Group, Universidad de Extremadura, Avda. Elvas s/n, E-06006 Badajoz, Spain
[b] Department of Chemistry, University of Southampton, Highfield, Southampton SO17 1BJ, UK

ARTICLE INFO

*Article history:*
Received 10 December 2010
Received in revised form 14 January 2011
Accepted 22 January 2011
Available online 28 January 2011

*Keywords:*
Imine–enamine tautomerism
Conformational analysis
Hidrazones

ABSTRACT

Schiff bases derived from 2-hydroxy-1-naphthaldehyde, or 1-hydroxy-2-naphthaldehyde, and different saturated *N*-aminoheterocycles have been prepared. Their structures have been elucidated in both solution and the solid state, including unequivocal X-ray diffraction analyses. Experimental data evidence the presence of imine (or hydrazone) structures as the most stable tautomers, while all attempts to switch to enamine (or enhydrazine) structures based on electronic and steric considerations were unsuccessful. A complete conformational analysis assisted by DFT calculations at B3LYP/6-31G* and M06-2X/6-311++G** levels has been performed on each series of representative structures.



## 1. Introduction

Schiff bases derived from aromatic *o*-hydroxy aldehydes, such as salicylidenanilines, may exist either as a single tautomer or a mixture of two in equilibrium: a *cis*-quinonoid structure (enamine or keto tautomer) characterized by an O···H–N intramolecular hydrogen bonding, and a benzenic structure (imine or enol tautomer) possessing the alternative O–H···N intramolecular bonding (Scheme 1). Such tautomers can be identified in both solutions through spectroscopic methods and the solid state by X-ray diffraction. It is generally assumed that the most stable tautomer of salicylidenanilines is the iminic form.[1] Zwitterionic structures having a longer $N^+$–H bond, have also been formulated,[2] though their diagnostic value is less important.


**Scheme 1.**

Salicylidenanilines exhibit remarkable photo- and thermo-chromic properties hinged on the molecular structure and markedly influenced by electronic interactions in the conjugated system (π–π and *n*–π) and steric effects.[3,4] In photochromic systems, salicylidenanilines adopt a non-planar conformation, favored by *n*–π interaction involving the lone pair on the nitrogen atom and the adjacent aromatic ring. In planar molecules stabilized by π–π interaction, the lone pair is not longer coupled to the aryl ring. As a result the intramolecular hydrogen bond is stronger and proton transfer may occur in the ground state, either at room temperature or upon heating (thermo-chromic behavior). Moreover, in the solid state photo- and thermo-chromic responses can be reversible and therefore imine–enamine equilibria, induced by UV radiation or heat, can be exploited in the fabrication of organic nanophotonic materials.[5]

Schiff bases generated from amines adopt a preferential tautomeric structure that largely depends on the parent carbonyl compound. While salicylaldehydes lead usually to imines, 2-hydroxy-1-naphthaldehyde gives rise to enamines. In contrast, Schiff bases generated from hydrazines produce hydrazones, which have invariably an iminic structure with the aforementioned aldehydes.[6] Thus, the structure of salicylaldazine (**1**), resulting from the reaction of salicylaldehyde and hydrazine, has been recently determined.[7,8] Since hydrazones derived from salicylaldehydes often exhibit a broad biological activity, a vast number of compounds have been synthesized, common derivatives arising from aryl hydrazines[9] and acyl hidrazides.[10] Particular cases include semicarbazones (**2**)[11] and

* Corresponding author. Tel.: +34 924289382; fax: +34 924271149; e-mail address: rmarvaz@unex.es (R.F. Martínez).

0040-4020/$ – see front matter © 2011 Elsevier Ltd. All rights reserved.
doi:10.1016/j.tet.2011.01.065

their thioanalogs (**3**).[12] Likewise, Schiff bases derived from 2-hydroxy-1-naphthaldehyde and hydrazines, acyl hydrazides (**4**–**7**), semicarbazones, and thiosemicarbazones (**8**) show an iminic structure in both solution and the solid state.[13] Compound **5** is an inhibitor of the DNA polymerase and HIV-reverse transcriptase RNase H.[14] Hydrazone **6** forms a fluorescent complex in the presence of Mg(II), thereby facilitating the determination of this ion in serum,[15] whereas a complex of **7** with Fe(II) exhibits antitumoral activity.[16] Hydrazones derived from 1-hydroxy-2-naphthaldehyde are less known, though they show equally a preferential enamine structure with amines and imine tautomers with hydrazines.

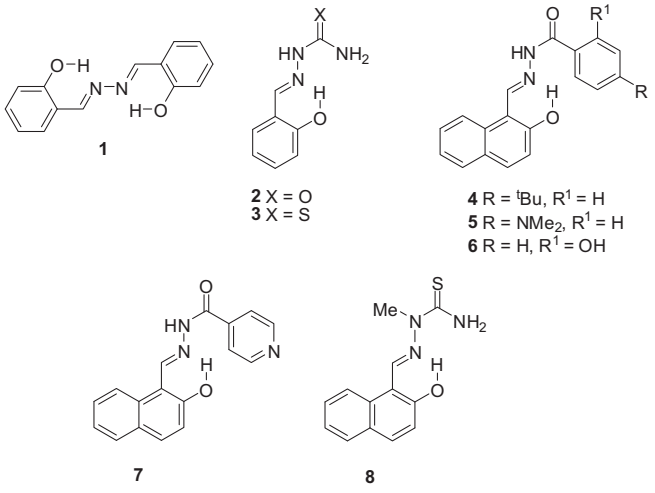


We could only find two antecedents dealing with enamine tautomers in hydrazones. Thus, chemiluminescence has been observed when a basic solution of hydrazone **9**, derived from salicylaldehyde, is irradiated with visible light. This causes isomerization of the inactive imine tautomer into enamine **10**.[17] In a second example, a hybrid hydrazone combining both aldehyde and acetophenone fragments, shows the two tautomeric forms (i.e., phenol–imine **11** and keto-enamine **12**) in the crystal unit cell.[18] Notably, the tautomeric behavior is associated to the acetophenone moiety, which contrasts with other hydrazones derived from *o*-hydroxyacetophenones lacking this phenomenon.[10b–e,19]

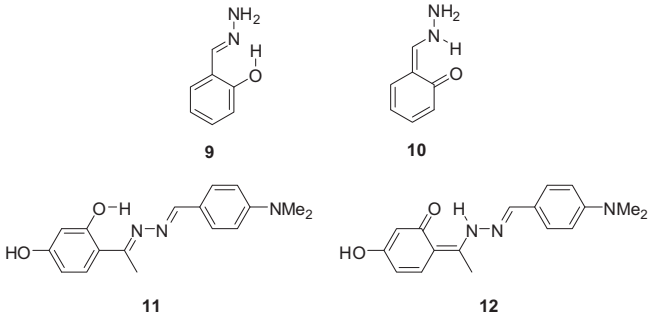


It is surprising that while Schiff bases derived from 2-hydroxy-1-naphthaldehyde adopt preferentially enamine structures, the corresponding hydrazones only exist as imines. The origin lies presumably in the existence of a lone pair on the nitrogen atom contiguous to the iminic nitrogen. The interaction of such a pair with the other lone pair on the iminic nitrogen or with π electrons from the carbon–nitrogen double bond may offer the clue to understand the salient preference of hydrazones to adopt the imine structure. Accordingly, three possibilities should be taken into account:

(a) an orthogonal disposition between the lone pairs on the nitrogen atoms. This arrangement avoids their interaction and each pair lies in a nodal plane of the other, as found in the most stable conformation of hydrazines.[20] Thus, the lone pair on the non-iminic nitrogen would be parallel to the p orbitals forming the π system of the C=N bond. There will be delocalization through that bond and the aromatic ring. Hydrazones possessing an imine structure will exhibit this molecular configuration (**13**);
(b) a coplanar disposition between the lone pairs, though in an antiperiplanar conformation (**14**) that minimizes the electronic repulsion;
(c) a coplanar disposition between the lone pairs, now adopting a synperiplanar conformation (**16**). In this case there will be a strong repulsion between the lone pairs; the so-called α-effect is attributed to this type of interactions.[21]

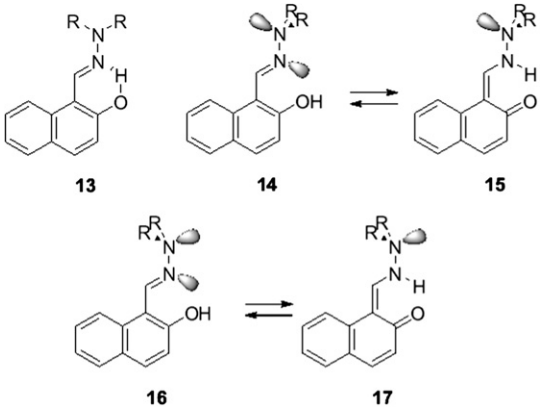


Arrangements, such as **14** and **16** could favor enamine structures (**15** or **17**), because proton transfer would eliminate the electronic repulsion by placing again the lone pairs in orthogonal orbitals.

As a result, one could also expect that Schiff bases bearing a lone pair on an atom vicinal to the iminic nitrogen would exhibit imine structures. The presence of appropriate R substituents in **13** could also favor preferential arrangements such as **14** or **16**, and therefore enamine structures **15** or **17**, respectively. Bulky groups will cause steric hindrance, thus avoiding the possibility of generating a structure like **13** and altering the electronic properties of the non-iminic heteroatom. This surmise will be scrutinized through the present manuscript.

## 2. Results and discussion

### 2.1. Synthesis of hydrazones

A series of hydrazones derived from 2-hydroxy-1-naphthaldehyde and the less studied 1-hydroxy-2-naphthaldehyde have been prepared, and fully characterized in both solution and the solid state. As mentioned above, this design is based on a rationale looking for structures with modified electronic properties. Thus, the syntheses of hydrazones **18**–**21** were accomplished to assess the effect of the conformations adopted by the heterocyclic ring on the electronic interactions. In a similar way compounds **22**–**25** derived from 1-hydroxy-2-naphthaldehyde, were obtained. The

presence of substituents at *ortho* positions in **21** and **25**, relative to **20** and **24**, respectively, could modify the interaction between the lone pairs on the hydrazone moiety.

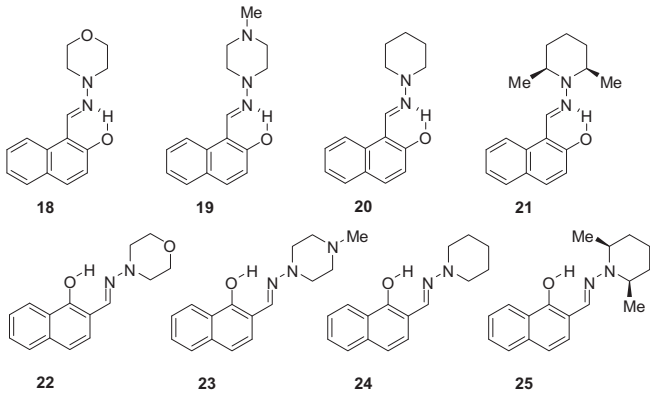


The experimental protocol involves the condensation of equimolar amounts of 2-hydroxy-1-naphthaldehyde (or 1-hydroxy-2-naphthaldehyde) with *N*-aminomorpholine, *N*-amino-*N*′-methylpiperazine, and *N*-aminopiperidine in ethanol at room temperature, which produces the corresponding hydrazones **18**–**25**[22] in variable, yet unoptimized, yields (Table 1).

**Table 1**
Chemical yields (%) and selected IR, $^{1}$H and $^{13}$C NMR data of compounds **18**–**25**

| Compound | Yield | $\nu_{C=N}$[a] | $\delta_{OH}$[b] | $\delta_{CH=N}$[b] | $\delta_{C-OH}$[b] | $\delta_{CH=N}$[b] |
|---|---|---|---|---|---|---|
| **18** | 58 | 1625 | 12.82 | 8.68 | 157.6 | 138.1 |
| **19** | 39 | 1622 | 12.93 | 8.61 | 157.5 | 137.9 |
| **20** | 47 | 1621 | 13.17 | 8.61 | 157.3 | 136.6 |
| **21** | 71 | 1623 | 13.94 | 9.27 | 163.2 | 160.2 |
| **22** | 73 | 1625 | 12.57 | 7.90 | 154.7 | 142.3 |
| **23** | 51 | 1629 | 12.73 | 7.84 | 154.5 | 141.5 |
| **24** | 25 | 1632 | 12.95 | 7.83 | 154.4 | 140.3 |
| **25** | 24 | 1629 | 13.43 | 8.37 | 163.0 | 162.8 |

[a] In $cm^{-1}$.
[b] In ppm.

## 2.2. Solid-state structures

Both elemental analyses and spectroscopic data are consistent with the proposed structures. Table 1 collects FT-IR absorptions and significant NMR resonances of the hydrazone fragment. The stretching band of the C=N bond at ~1625 $cm^{-1}$, along with its low intensity, suggest an imine structure.[23a] The carbonyl group in an alternative enamine disposition will also exhibit a similar absorption, although much more intense due to the increased polarity of that bond.[23b]

Unequivocal solid-state structures could further be confirmed through X-ray diffraction analyses of compounds **18**, **20**, and **23** whose ORTEP diagrams are depicted in Fig. 1.[24]

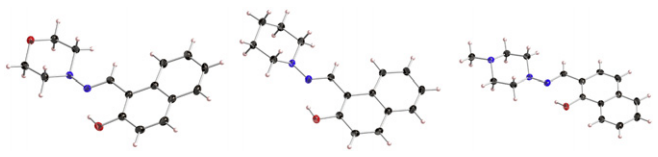

**Fig. 1.** Solid-state structure of **18**, **20**, and **23** with thermal elipsoids drawn at 35% probability.

In all the cases, there is an intramolecular hydrogen bond between the phenolic OH group and the iminic nitrogen, as evidenced by short O···N distances (Table 2). Thus, the length of the C–O bond is 1.350 Å for **18**, 1.358 Å for **20**, and 1.353 Å in **23**, which are consistent with a single bond; while the C=N bond distance is 1.292 Å in both **18** and **23**, and 1.294 Å in the case of **20**. The mean plane of the heterocyclic ring is approximately coplanar with the naphthylmethylene fragment.

**Table 2**
Intramolecular hydrogen bonds present in **18**, **20**, and **23** (Å and °)

| Compound | $d(D-H)$ | $d(H\cdots A)$ | $d(D\cdots A)$ | $\angle(DHA)$ |
|---|---|---|---|---|
| **18** | 0.84 | 1.83 | 2.575 (2) | 146.7 |
| **20** | 0.84 | 1.85 | 2.585 (2) | 146.0 |
| **23** | 0.84 | 1.86 | 2.598 (2) | 146.0 |

## 2.3. Structure in solution

$^{1}$H and $^{13}$C NMR spectra show signals consistent with a phenol–imine structure; the iminic proton and the phenol OH group appear as singlets, with the phenolic carbon resonating in most cases at ~157 ppm. In an alternative enamine structure, one should expect the coupling between the protons present in that functionality as well as a carbonyl group resonating at ~170 ppm.

In these substances the aromatic fragment is coplanar with the hydrazone moiety; so we were particularly interested in compounds **21** and **25**, as one could expect deviations from coplanarity due to the steric hindrance caused by methyl groups at C-2 and C-6 at the piperidine ring. This would likewise modify the relative disposition of the lone pairs on both nitrogen atoms, thus enabling a keto-amine structure. However, $^{1}$H and $^{13}$C NMR spectra of both **21** and **25** showed only signals compatible with a phenol–iminic arrangement, although chemical shifts appeared to be relatively deshielded with respect to those of **20** and **24** ($\Delta\delta_{OH}$ in the range 0.77–0.48 ppm, $\Delta\delta_{=CH}$: 0.66–0.54 ppm, $\Delta\delta_{CO}$: 5.9–8.6 ppm, and $\Delta\delta_{C=N}$: 23.6–22.5 ppm), owing to conformational changes caused by steric effects. The change however had no effect on the imine structure.

## 2.4. Computational calculations and conformational analysis

To shed light into the steric effects on the structure and conformation of **21** and **25**, compounds **20** and **21**, as representative examples, were analyzed together with their possible tautomeric forms **26** and **27**, respectively.

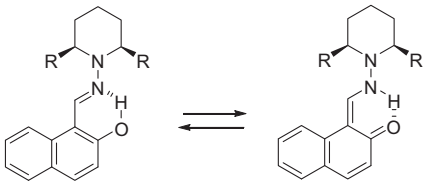


The conformational profile resulting from rotation around the N–N bond was obtained by means of DFT calculations at the B3LYP/6-31G* level[25] using Gaussian09 package.[26] To this end and starting from a conformation of minimal energy, we have calculated the energy of molecular arrangements obtained by successive 15°-rotations around the N–N bond ($\theta_{C-N-N-C}$) without any further geometrical restriction in gas phase. Then, it has been determined the geometry corresponding to conformational minima and maxima, which represent the transition structures involving interconversion between

the most stable conformations. Such transition states were characterized by their unique imaginary frequency. Recently, Zhao and Truhlar[27] have recommended the use of an alternative functional, M06-2X, for main-group thermochemistry, barrier heights, and for the study of noncovalent interactions such as intramolecular hydrogen bonding. Bearing this premise in mind, the free energies calculated at the B3LYP/6-31G* level have now been re-assessed at the M06-2X/6-311++G** level with complete geometry optimization as well. Moreover and, although there are no anions, the inclusion of diffuse functions to accurately model the hydrogen bond appeared to be more convenient. In addition, the role of solvent has been taken into account through the SMD[28] model. To check the influence of polarity, calculations have been performed in $CHCl_3$ ($\varepsilon$=4.7), the solvent employed for recording NMR spectra, as well as DMSO ($\varepsilon$=46.8). However, the results obtained are quite similar (see Tables 3–6) and, accordingly, the discussion concentrates only on the former.

**Table 3**
Conformational data of **20** (angles are given in degrees and energies in kcal mol$^{-1}$)

| | Minima | | Maxima | |
|---|---|---|---|---|
| Conformer | **20a** | **20c** | **20b** | **20d** |
| Dihedral angle[a] | 13.5 | 210.3 | 123.6 | 295.3 |
| $\Delta G_r$[a,b] | 0.00 | 0.00 | 2.59 | 9.25 |
| Dihedral angle[c] | 16.2 | 210.6 | 122.6 | 296.7 |
| $\Delta G_r$[b,c] | 0.00 | 0.00 | 3.15 | 8.52 |
| Dihedral angle[d] | 16.2 | 211.2 | 121.2 | 297.1 |
| $\Delta G_r$[b,d] | 0.00 | 0.00 | 4.01 | 7.75 |

[a] At the B3LYP/6-31G* level.
[b] Relative free energy with respect to that of **20a** or **20c**.
[c] At the M06-2X/6-311++G** level, including the solvent effect (SMD model, $CHCl_3$ as solvent).
[d] At the M06-2X/6-311++G** level, including the solvent effect (SMD model, DMSO as solvent).

**Table 4**
Conformational data of **26** (angles given in degrees and energies in kcal mol$^{-1}$)

| | Minima | | Maxima | |
|---|---|---|---|---|
| Conformer | **26b** | **26d** | **26a** | **26c** |
| Dihedral angle[a] | 119.8 | 295.2 | 42.9 | 192.2 |
| $\Delta G_r$[a,b] | 1.40 | 5.57 | 8.14 | 8.14 |
| Dihedral angle[c] | 119.2 | 296.5 | 41.7 | 194.6 |
| $\Delta G_r$[b,c] | 2.78 | 7.53 | 8.33 | 8.33 |
| Dihedral angle[d] | 119.2 | 296.7 | 44.0 | 192.6 |
| $\Delta G_r$[b,d] | 2.64 | 6.56 | 7.94 | 7.94 |

[a] At the B3LYP/6-31G* level.
[b] Values relative to **20a**/**20c**.
[c] At the M06-2X/6-311++G** level, including the solvent effect (SMD model, $CHCl_3$ as solvent).
[d] At the M06-2X/6-311++G** level, including the solvent effect (SMD model, DMSO as solvent).

**Table 5**
Conformational data of **21** (angles are given in degrees and energies in kcal mol$^{-1}$)

| | Minima | | | Maxima | | |
|---|---|---|---|---|---|---|
| Conformer | **21a** | **21b** | **21c** | **21e** | **21f** | **21d** |
| Dihedral angle[a] | 10.8 | 116.8 | 202.3 | 46.6 | 180.3 | 294.8 |
| $\Delta G_r$[a,b] | 4.67 | 0.00 | 4.67 | 7.88 | 7.88 | 8.39 |
| Dihedral angle[d] | 7.1 | 115.3 | 211.6 | 43.7 | 185.7 | 296.2 |
| $\Delta G_r$[c,d] | 3.89 | 0.07 | 3.89 | 7.27 | 7.27 | 18.24 |
| Dihedral angle[e] | 6.3 | 117.2 | 213.5 | 44.1 | 185.7 | 298.7 |
| $\Delta G_r$[b,e] | 4.12 | 0.00 | 4.12 | 8.08 | 8.08 | 13.95 |

[a] At the B3LYP/6-31G* level.
[b] Values relative to **21b**.
[c] Values relative to **27b**.
[d] At the M06-2X/6-311++G** level, including the solvent effect (SMD model, $CHCl_3$ as solvent).
[e] At the M06-2X/6-311++G** level, including the solvent effect (SMD model, DMSO as solvent).

**Table 6**
Conformational data of **27** (angles in degrees and energies in kcal mol$^{-1}$)

| | Minima | | Maxima | |
|---|---|---|---|---|
| Conformer | **27b** | **27d** | **27a** | **27c** |
| Dihedral angle[a] | 119.8 | 294.7 | 42.5 | 184.8 |
| $\Delta G_r$[a,b] | 0.23 | 3.88 | 12.94 | 12.94 |
| Dihedral angle[d] | 118.2 | 295.9 | 38.1 | 193.3 |
| $\Delta G_r$[c,d] | 0.00 | 2.34 | 13.02 | 13.02 |
| Dihedral angle[e] | 118.0 | 296.2 | 39.1 | 192.7 |
| $\Delta G_r$[b,e] | 0.37 | 4.03 | 12.66 | 12.66 |

[a] At the B3LYP/6-31G* level.
[b] Values relative to **21b**.
[c] Values relative to **27b**.
[d] At the M06-2X/6-311++G** level, including the solvent effect (SMD model, $CHCl_3$ as solvent).
[e] At the M06-2X/6-311++G** level, including the solvent effect (SMD model, DMSO as solvent).

## 2.5. Tautomers 20/26

Data corresponding to tautomers **20** and **26** are collected in Fig. 2 and Tables 3 and 4.

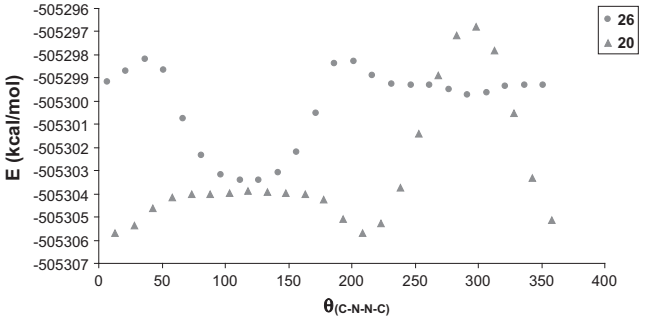


**Fig. 2.** Conformational profile for tautomeric compounds **20** and **26** (B3LYP/6-31G* level).

Hydrazone **20** shows two enantiomeric conformations of minimum energy **20a** and **20c** (at $\theta$ values of ~16° and ~211°, respectively) and two transition states, **20b** and **20d** (at $\theta$ values of ~123° and ~297°, respectively), which correspond to the two possible interconversion routes by rotation, though with different energy (Fig. 3). Both minima can be represented by a structure, such as **13**, for which the lone pairs on the two nitrogen atoms lie approximately in an orthogonal disposition.

The transition structures are reached when the conformational minima rotate ~90° around the N–N bond. The higher in energy, **20d**, corresponds to a disposition like **16**, for which the angle between the lone pair is close to 0°. This arrangement generates a strong repulsive interaction that, together with the steric interactions involving the iminic proton and the axial hydrogens at C-2 and C-6 of the piperidine ring, contribute to destabilize such a structure in ~8 kcal mol$^{-1}$. In stark contrast, the lone pairs form an angle of ~180° in the lowest transition structure, **20b**, which corresponds to the structure represented by **14**. In this disposition the repulsive interaction is smaller with a destabilization of less than 3.2 kcal mol$^{-1}$. Overall, the energy difference between both transition states is ~5.4 kcal mol$^{-1}$ and suggests that the transformation involving the most stable conformations chiefly occurs by bending through the lower maximum ($\theta$ ~123°): **20a**↔**20b**↔**20c**.

Another possible pathway for interconversion to occur would involve nitrogen inversion at the piperidine ring along with, in a concomitant or sequential process, chair inversion of the six-membered heterocycle. In this way **20a** and **20c** may interconvert as well as **20b** into **20d**. However, this route should overcome

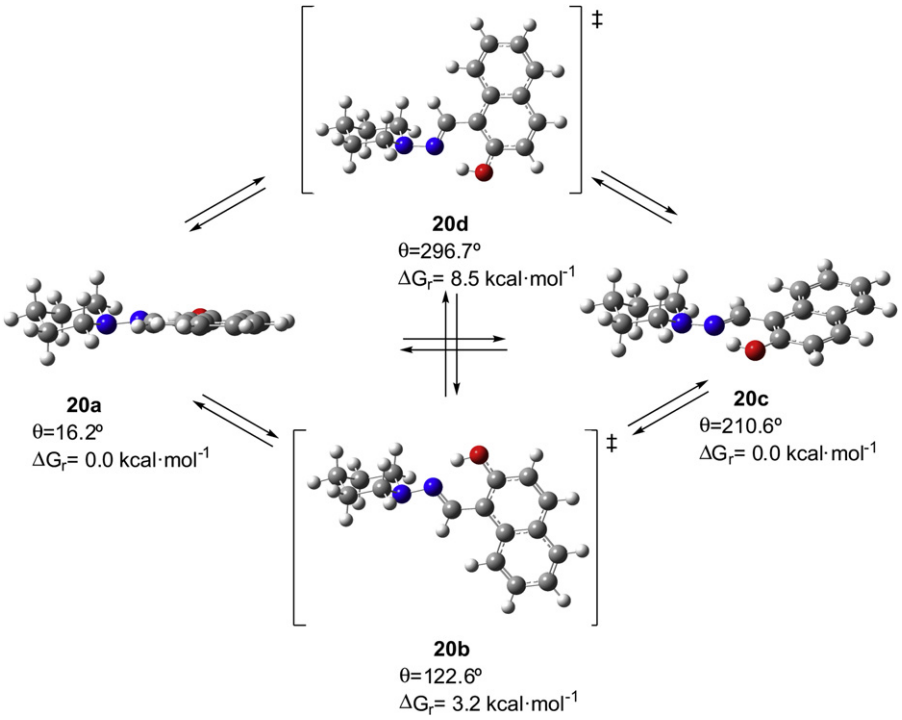


**Fig. 3.** Optimized structures (M06-2X/6-311++G** level) in $CHCl_3$ as solvent (SMD model) of the most stable conformers and transition structures of **20** (the relative free energies, $\Delta G_r$, are referred to **20a**/**20c**).

a significant energy barrier, which in the case of piperidine has been estimated to be 10.4 kcal $mol^{-1}$ for chair conformational reversal barrier, and 6.1 kcal $mol^{-1}$ for nitrogen inversion barrier.[29,30]

The conformational behavior of tautomer **26** is completely different to that of **20** (Table 4, Fig. 4). The most stable conformers, **26b** and **26d** (observed at $\theta$ values of ~119° and ~297°, respectively), take place at those $\theta$ values measured for the transition structures **20b** and **20d**, while the enantiomeric maxima **26a** and **26c** (at $\theta$ ~42° and ~195°, respectively), exhibit $\theta$ values that are approximately coincidental with those observed for the conformational minima **20a** and **20c**.

It is obvious that proton transfer converts the conformational maxima **20d** and **20b** into conformers **26d** and **26b**, because the repulsion between the lone pairs is alleviated moving from angles at ~0° and ~180° in the first cases to a final value of 90°. Accordingly **26a** and **26c** become maxima, although the interaction involves the lone pair of the $sp^3$-hybridized piperidine nitrogen and one pair of the $sp^2$-hybridized imine nitrogen, which is also

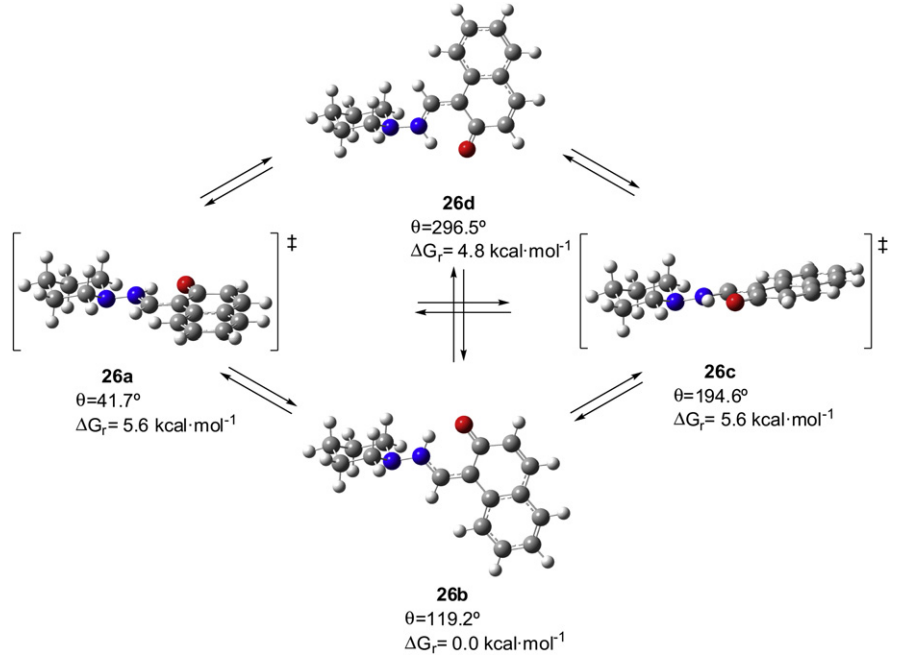


**Fig. 4.** Optimized structures (at the M06-2X/6-311++G** level) in $CHCl_3$ as solvent (SMD model) for the most stable conformers and transition structures of **26** ($\Delta G_r$ refers to **26b**).

involved in conjugation with the aromatic ring. Overall, the situation is intermediate between the electronic arrangements in **20b** (equivalent to **14**) and **20d** (equivalent to **16**); in fact the relative energy ($\Delta G_r$) for **26a**/**26c** (5.6 kcal mol$^{-1}$) agrees well with the arithmetic mean of the energy values for **20b** and **20d**, (3.15+8.52)/2=5.83 kcal mol$^{-1}$.

The above results evidence that for enamine structures to occur, the corresponding hydrazone should adopt molecular dispositions, such as **15** or **17**, for which the substituents at the non-iminic nitrogen lie in a perpendicular plane to the rest of the molecule while the lone pairs on both nitrogens form a dihedral angle of ~90°.

Nevertheless, the computational calculations reveal the greater stability of imine structures (**20a**/**20c**) than the enamine tautomer **26b** by ~2.7 kcal mol$^{-1}$, which agrees with the experimental result.

Through and NBO analysis[31] we have further evaluated the influence of the second-order stabilizing interactions of the lone pairs, at both nitrogen atoms, on the conformations **20a**–**d** (Fig. 5, Table 1S in Supplementary data). The two interactions of LP36 with $\sigma^*_{C10-H26}$ and $\sigma^*_{C16-H34}$ (~6–8 kcal mol$^{-1}$), that is, those involving the bonds of axial hydrogens on carbons vicinal to the nitrogen atom in $^4C_1$ disposition, remain in all conformations of **20** and **26**.

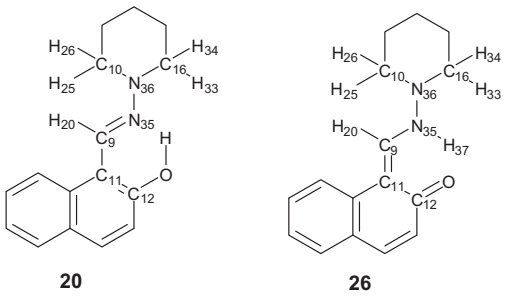


**Fig. 5.** Atom numbering for the NBO analysis.

wIn the most stable conformers of **20**, **20a**, and **20c**, the most important interaction involves the lone pair on nitrogen from the piperidine fragment (LP36) and the $\pi^*$ orbital of the C9–N35 bond (25.2 kcal mol$^{-1}$). This interaction favors an orthogonal arrangement between the lone pairs of both nitrogens. Other important interactions take place between the lone pairs of the iminic nitrogen (LP35) and the $\sigma^*$ orbital of contiguous bonds that lie in an antiperiplanar disposition relative to the former, i.e., LP35 with $\sigma^*_{C9-H20}$ and $\sigma^*_{C10-N36}$ (9.75 and 8.74 kcal mol$^{-1}$, respectively); the latter favoring a quasi-orthogonal arrangement between the lone pairs of both nitrogens.

In conformer **20b**, for which both lone pairs adopt an antiperiplanar disposition, the strong interaction of LP36 with $\pi^*_{C9-N35}$ present in **20a**/**20c** disappears, while it is considerably reduced in **20d**, for which both pairs are essentially eclipsed (5.45 kcal mol$^{-1}$).

Both **26a**/**26c** and **26d** show a strong interaction between the lone pair on the enamine nitrogen (LP35) and the $\pi^*_{C9-C11}$ orbital (>60 kcal mol$^{-1}$), whereas in contrast **26b** exhibits a rather modest interaction between the lone pair on the piperidine nitrogen and the $\sigma^*$ orbital corresponding to the NH bond (7.68 kcal mol$^{-1}$).

### 2.6. Tautomers 21/27

Compound **21** with an imine structure shows a conformational profile completely different to that of imine **20** and similar to enamine **26** instead. The behavior is however complex showing three minima and three maxima; in the $\theta$ range between 0° and 200° the patterns observed for **21** and **26** are almost coincidental. The most striking difference is the existence of a maximum at ~296° (**21d**) while **26d** shows a minimum (Fig. 6, Table 5).

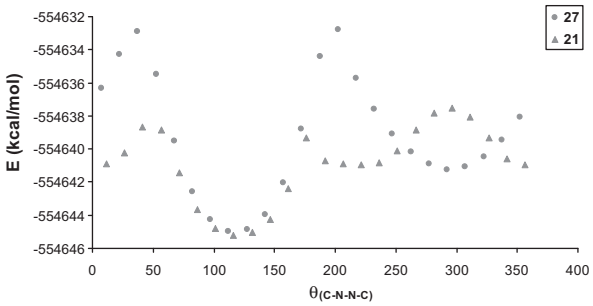


**Fig. 6.** Conformational profile for compounds **21** and **27** (B3LYP/6-31G* level).

It is obvious that conformational differences between **20** and **21** should reasonably ascribed to steric effects caused by the two methyl groups at C-2 and C-6 in the piperidine ring, because the interactions involving the lone pairs on both nitrogen atoms remain unaffected. In fact the geometries of conformers **21a**–**d** are identical to those of **20a**–**d**, although the relative energies of **21a** and **21c** increase due to steric hindrance, thus converting **21b** into the most stable conformer (Fig. 7). The point something new is the appearance of two maxima, one intermediate between **21a** and **21b** at $\theta$ ~44° (**21e**) and another between **21b** and **21c** at $\theta$ ~186° (**21f**).

However, the conformational behavior of enamine **27** is quite similar to that of **26**; the geometries of the two stable conformers and the corresponding transition states of the former are essentially coincidental with those observed for the latter (Table 6, Fig. 8). A striking difference is the fact that rotation barriers for **27** are considerably greater than those of **26**; which can be attributed not only to the steric effects present in **27a** and **27c**, but also to the interaction between the lone pairs. Thus, the calculated barrier (13.0 kcal mol$^{-1}$) corresponds with the sum of the energy differences between **21e**–**b**, which account for the steric effects, and **26a**,**b**, which evaluate the lone pair interaction (7.2+5.6=12.8 kcal mol$^{-1}$).

Remarkably, the conformational profiles of **21** and **27** are essentially identical for $\theta$ values from 75° to 180°. Accordingly, the energy difference between the most stable structures, i.e., imine **21b** and enamine **27b**, is almost negligible ($\Delta\Delta G_r$=0.07 kcal mol$^{-1}$), since there is no appreciable change in their geometry as evidenced by the small variation of the dihedral angle (~3°). In spite of this computational estimation, experimental analyses do not detect any enamine structure in solution for compounds **20** and **21** at room temperature. Further inspection by variable-temperature NMR monitoring, cooling from 298 to 220 K, did not reveal the presence of any enamine tautomer either.

The methyl groups at C-2 and C-6 of the piperidine ring ($^4C_1$ conformation) adopt an equatorial disposition that minimizes steric interactions. The NBO analysis (Table 2S in Supplementary data) reveals that conformers **21a**–**e** exhibit an appreciable interaction between the piperidine lone pair (LP36) and the $\sigma^*$ orbitals of the CH bonds at C-2 and C-6, whose axial disposition place them in an *anti* arrangement relative to LP36 (~4.5–7.5 kcal mol$^{-1}$) (Fig. 9). Nevertheless, the most important interaction of LP36 involves the $\pi^*$ orbital of the C9-N35 double bond in conformers **21a**/**21c** (~30 kcal mol$^{-1}$); this interaction being reduced in **21e** and **21f** (~20 kcal mol$^{-1}$) and disappearing completely in **21b**.

The lone pair of the iminic nitrogen (LP35) shows an appreciable interaction with the $\sigma^*$ orbital of all bonds bearing an *anti* disposition. This occurs with the imine CH bond (C9–H20) in the whole range of conformers (~8–10 kcal mol$^{-1}$) and the C10–N36 (or C16–N36) bond in conformers **21a**/**21c** (8.4 kcal mol$^{-1}$) and **21f** and **21e** (5.2 kcal mol$^{-1}$). It is worth noting the existence of a strong interaction of LP35 with the $\sigma^*$ orbital of the hydroxyl bond ($\sigma^*_{O42-H43}$), which is only present in **21e** and **21f** (~35 kcal mol$^{-1}$).

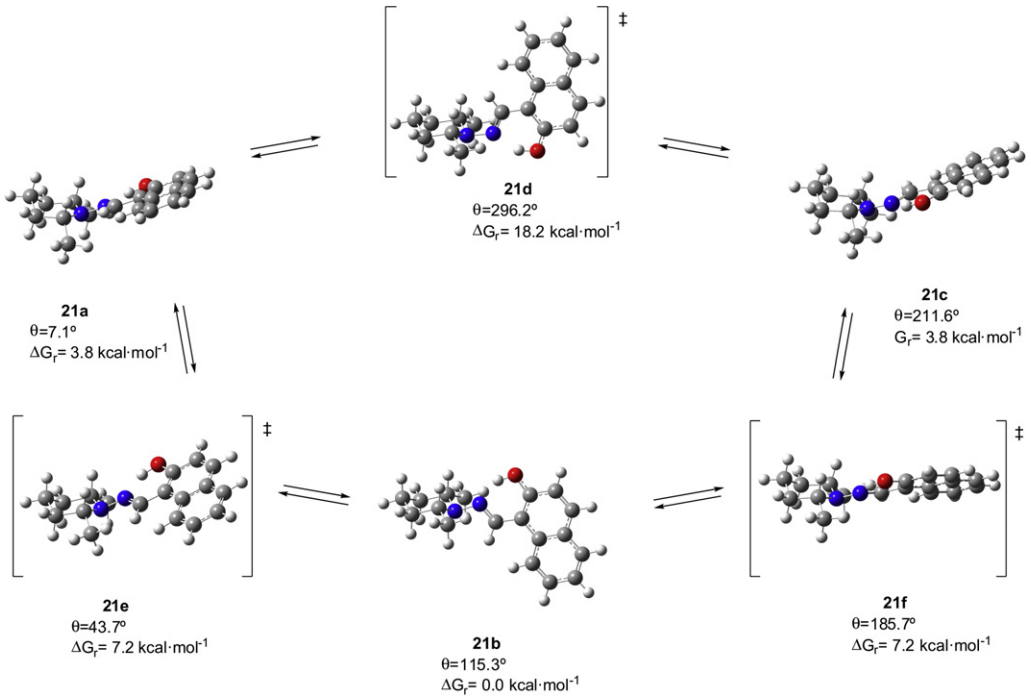


**Fig. 7.** Optimized structures (at the M06-2X/6-311++G** level) in $CHCl_3$ as solvent (SMD model) for the most stable conformers and transition states of **21** ($\Delta G_r$ is referred to **21b**).

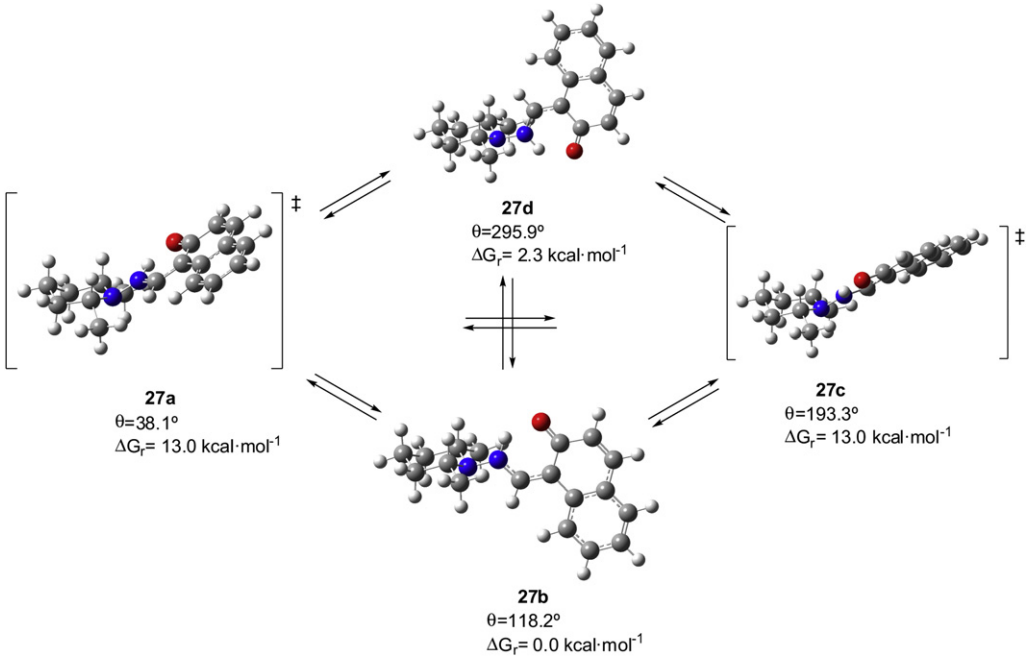


**Fig. 8.** Optimized structures (at the M06-2X/6-311++G** level) in $CHCl_3$ as solvent (SMD model) of the most stable conformers and transition states of **27** ($\Delta G_r$ is referred to **27b**).

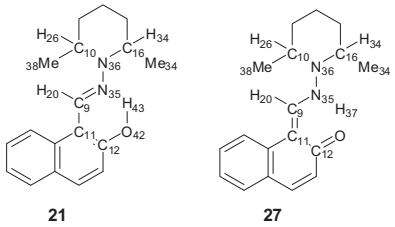


**Fig. 9.** Atom numbering for the NBO analysis.

The NBO analysis for the entire range of conformers of **27** reveals that the most important interactions involve the lone pair on the enamine nitrogen (LP35) and the $\pi^*$ orbital of the C9–C11 double bond in **27a**/**27c** (~67 kcal mol$^{-1}$).

## 2.7. Imine–enamine tautomerization

We have further evaluated the imine–enamine interconversion by calculating the activation energy for that process in the cases of **20**/**26** and **21**/**27**.

For the first couple, the activation energy ($\Delta G^{\ddagger}$) found for the tautomerization between the most stable conformers, i.e., **20a**/**20c** and

**26b**, is 5.55 kcal mol$^{-1}$ at M06-2X/6-311++G** level in $CHCl_3$ as solvent (4.99 kcal mol$^{-1}$ in DMSO); which is low enough to ensure a rapid interconversion at room temperature. The structure of the transition state corresponds to a proton-transfer process that converts imines **20a**/**20c** to enamine **26a** (Fig. 10a). A further rotation of ~90° eliminates the lone pair interaction on both nitrogens leading to **26b**.

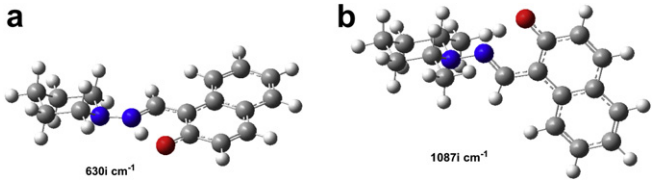


**Fig. 10.** Structures of the transition states associated with the conversions of: (a) **20a**/**20c** to **26b** through **26a**, and (b) **21b** to **27b** (at the M06-2X/6-311++G** level in $CHCl_3$ as solvent, SMD model).

The transformation of **21b** into **27b** only involves proton transfer (Fig. 10b), because both forms exhibit a quite similar geometry and the resulting activation energy ($\Delta G^{\ddagger}$) is 1.29 kcal mol$^{-1}$ at M06-2X/6-311++G** level in $CHCl_3$ as solvent (1.78 kcal mol$^{-1}$ in DMSO).

## 3. Conclusions

The above study introduces a systematic exploration of hydrazones derived from hydroxynaphthaldehydes and primary hidrazines. Experimental data support the exclusive formation of imine structures. Computational calculations have been carried out on the different conformers and transition structures involved in the tautomerization process. Such results clearly evidence the particular geometry requirements for either imine or enamine structures to exist in hydrazones derived from *o*-hydroxy arylaldehydes. Likewise, the conformational inspection reveals that either Schiff base derived from an *o*-hydroxy arylaldehyde bearing a lone pair on the atom adjacent to the iminic nitrogen will preferentially adopt an imine structure. This predictive behavior should be corroborated in further studies, such as those involving oxime derivatives. Although computational calculations were initially considered at the common B3LYP/6-31G* level, recent evaluations of DFT methods have evidenced some minuses, especially to model weak interactions, such as hydrogen bonds. Thus, this study has now included further inspection of free energies and geometries at higher level of theory: M06-2X/6-311++G**, and taken into consideration solvents effect as well (through the SMD model). However, similar statements can be inferred from both calculations, thus evidencing the robustness of DFT methods as well as the little or no influence of polarity effects.

## 4. Experimental section

### 4.1. General

Melting points were determined on Gallenkamp and Electrothermal apparatuses and are uncorrected. IR spectra were recorded in the range of 4000–600 cm$^{-1}$ on an FT-IR THERMO spectrophotometer. Solid samples were recorded on KBr (Merck) pellets. NMR spectra were recorded on Bruker 400 and 500 AC/PC instruments, in different solvent systems. Assignments were confirmed by homo- and hetero-nuclear double-resonance and DEPT (distortionless enhancement by polarization transfer). TMS was used as the internal standard ($\delta$=0.00 ppm) and all *J* values are given in hertz. Microanalyses were determined on a Leco 932 analyser.

### 4.2. X-ray data collection and structural refinement

Cell dimensions and intensity data for **18**, **20** were recorded at 120 K, using a Bruker Nonius KappaCCD area detector diffractometer mounted at the window of a rotating Mo anode ($\lambda$ (Mo K$\alpha$)=0.71073Å). Data collection and processing were carried out using the programs COLLECT[32] and DENZO[33] and an empirical absorption correction was applied using SADABS.[34]

The structures were solved via direct methods[35] and refined by full matrix least squares on $F^2$. Maximum, minimum peaks (e Å$^{-3}$) in the final difference Fourier synthesis were found as 0.28, −0.21 (**18**); 0.19, −0.25 (**20**); and 0.31, −0.33 (**23**), respectively. The hydrogen atoms in both structures were placed in calculated positions and included in the refinement using a riding model approximation. The hydroxyl hydrogens atoms were first located in the difference map and then included in the refinement using a riding model, the torsion angle was allowed to refine and in all cases matched the position identified in the difference map. Crystallographic illustrations were prepared using the CAMERON programs.[36] The molecular structures are shown in Fig. 1.

### 4.3. General procedure

To a solution of the amine (2.90 mmol) in ethanol (10 mL) was slowly added a solution of the corresponding aldehyde (2.90 mmol) in a small volume of methanol. The mixture was stirred at room temperature giving rise to a precipitate within a few minutes. When the mixture did not precipitate spontaneously, it was evaporated in vacuum and gave a solid on standing or on cooling. The resulting product was collected by filtration, washed successively with cold water, ethanol, and diethyl ether, and recrystallized from ethanol or methanol.

*4.3.1. 4-[(2-Hydroxy-1-naphthylmethylen)amino]morpholine (**18**).* From 2-hydroxy-1-naphthaldehyde and 4-aminomorpholine (58%); mp 124–125 °C, IR ($\nu$, KBr): 1625 (CH=N), 1593, 1515, 1471 cm$^{-1}$ (arom). $^1$H NMR (400 MHz, $CDCl_3$): $\delta$ 12.82 (1H, s, OH), 8.68 (1H, s, CH=N), 8.02 (1H, d, *J*=8.8 Hz, H-arom), 7.80 (1H, d, *J*=8.0 Hz, H-arom), 7.74 (1H, d, *J*=8.8 Hz, H-arom), 7.52 (1H, dd, *J*=6.8, 8.0 Hz, H-arom), 7.36 (1H, dd, *J*=6.8, 8.0 Hz, H-arom), 7.23 (1H, d, *J*=8.8 Hz, H-arom), 3.95 (4H, t, *J*=4.8 Hz, $CH_2$), 3.25 (4H, t, *J*=4.8 Hz, $CH_2$). $^{13}$C NMR (100 MHz, $CDCl_3$): $\delta$ 157.6 (C–OH), 138.1 (CH=N), 131.8, 131.3, 129.1, 128.2, 127.0, 123.1, 119.9, 119.2, 108.9 (C-arom), 66.2 ($CH_2$), 52.3 ($CH_2$). Anal. Calcd for $C_{15}H_{16}N_2O_2$: C, 70.29; H, 6.29; N, 10.93. Found: C, 70.36; H, 6.47; N, 10.93.

*4.3.2. 1-[(2-Hydroxy-1-naphthylmethylen)amino]-4-methylpiperazine (**19**).* From 2-hydroxy-1-naphthaldehyde and 1-amino-4-methylpiperazine (39%); mp 98–99 °C, IR ($\nu$, KBr): 1622 (CH=N), 1599, 1515, 1470, 1449 cm$^{-1}$ (arom). $^1$H NMR (400 MHz, $CDCl_3$): $\delta$ 12.93 (1H, s, OH), 8.61 (1H, s, CH=N), 8.03 (1H, d, *J*=8.4 Hz, H-arom), 7.78 (1H, d, *J*=8.0 Hz, H-arom), 7.73 (1H, d, *J*=8.8 Hz, H-arom), 7.50 (1H, m, H-arom), 7.35 (1H, t, *J*=7.6 Hz, H-arom), 7.21 (1H, d, *J*=8.8 Hz, H-arom), 3.31 (4H, t, *J*=5.0 Hz, $CH_2$), 2.70 (4H, t, *J*=5.2 Hz, $CH_2$), 2.41 (3H, s, $CH_3$). $^{13}$C NMR (100 MHz, $CDCl_3$): $\delta$ 157.5 (C–OH), 137.9 (CH=N), 131.7, 130.9, 129.1, 128.2, 126.9, 123.0, 119.9, 119.2, 109.1 (C-arom), 54.1 ($CH_2$), 51.4 ($CH_2$), 45.9 ($CH_3$). Anal. Calcd for $C_{16}H_{19}N_3O$: C, 71.35; H, 7.11; N, 15.60. Found: C, 71.50; H, 7.19; N, 15.56.

*4.3.3. 1-[(2-Hydroxy-1-naphthylmethylen)amino]piperidine (**20**).* From 2-hydroxy-1-naphthaldehyde and 1-aminopiperidine (47%); mp 95–96 °C, IR ($\nu$, KBr): 1621 (CH=N), 1597, 1519, 1467 cm$^{-1}$ (arom). $^1$H NMR (400 MHz, $CDCl_3$): $\delta$ 13.17 (1H, s, OH), 8.61 (1H, s, CH=N), 8.05 (1H, d, *J*=8.4 Hz, H-arom), 7.79 (1H, d, *J*=8.0 Hz, H-arom), 7.72 (1H, d, *J*=8.8 Hz, H-arom), 7.50 (1H, dt, *J*=1.2, 8.0 Hz, H-arom), 7.35 (1H, t, *J*=7.2 Hz, H-arom), 7.23 (1H, d, *J*=8.8 Hz, H-arom), 3.24 (4H, t, *J*=5.6 Hz, $CH_2$), 1.84 (4H, m, $CH_2$), 1.61 (2H, m, $CH_2$). $^{13}$C NMR (100 MHz, $CDCl_3$): $\delta$ 157.3 (C–OH), 136.6

(CH=N), 131.7, 130.5, 129.0, 128.2, 126.7, 122.9, 120.0, 119.2, 109.5 (C-arom), 52.5 ($CH_2$), 24.9 ($CH_2$), 23.9 ($CH_2$). Anal. Calcd for $C_{16}H_{18}N_2O$: C, 75.56; H, 7.13; N, 11.01. Found: C, 75.76; H, 7.08; N, 10.92.

*4.3.4. 2,6-Dimethyl-1-[(2-hydroxy-1-naphthylmethylen)amino]piperidine (**21**).* From 2-hydroxy-1-naphthaldehyde and 1-amino-2,6-dimethylpiperidine (71%); mp 71–72 °C, IR ($\nu$, KBr): 1623 (CH=N), 1577, 1515, 1472 $cm^{-1}$ (arom). $^1H$ NMR (400 MHz, $CDCl_3$): $\delta$ 13.94 (1H, s, OH), 9.27 (1H, s, CH=N), 8.05 (1H, d, $J$=8.4 Hz, H-arom), 7.77 (2H, m, H-arom), 7.53 (1H, t, $J$=7.8 Hz, H-arom), 7.35 (1H, t, $J$=7.4 Hz, H-arom), 7.19 (1H, d, $J$=8.8 Hz, H-arom), 2.87 (2H, s, CH), 1.79 (3H, s, $CH_2$), 1.52 (3H, s, $CH_2$), 1.06 (6H, s, $CH_3$). $^{13}C$ NMR (100 MHz, $CDCl_3$): $\delta$ 163.2 (C–OH), 160.2 (CH=N), 133.9, 132.9, 129.0, 127.7, 127.6, 123.2, 120.1, 119.7, 107.1 (C-arom), 60.0 (CH), 33.3 ($CH_2$), 23.5 ($CH_2$), 21.4 ($CH_3$). Anal. Calcd for $C_{18}H_{22}N_2O$: C, 76.56; H, 7.85; N, 9.92. Found: C, 76.50; H, 7.93; N, 9.99.

*4.3.5. 4-[(1-Hydroxy-2-naphthylmethylen)amino]morpholine (**22**).* From 1-hydroxy-2-naphthaldehyde and 4-aminomorpholine (73%); mp 131–132 °C, IR ($\nu$, KBr): 1625 (CH=N), 1581, 1562, 1448 $cm^{-1}$ (arom). $^1H$ NMR (400 MHz, $CDCl_3$): $\delta$ 12.57 (1H, s, OH), 8.35 (1H, m, H-arom), 7.90 (1H, s, CH=N), 7.75 (1H, m, H-arom), 7.49 (2H, m, H-arom), 7.34 (1H, d, $J$=8.4 Hz, H-arom), 7.23 (1H, d, $J$=8.8 Hz, H-arom), 3.93 (4H, t, $J$=4.8 Hz, $CH_2$), 3.20 (4H, t, $J$=4.8 Hz, $CH_2$). $^{13}C$ NMR (100 MHz, $CDCl_3$): $\delta$ 154.7 (C–OH), 142.3 (CH=N), 134.2, 127.4, 127.3, 126.4, 125.3, 125.0, 122.9, 118.6, 111.7 (C-arom), 66.1 ($CH_2$), 52.1 ($CH_2$). Anal. Calcd for $C_{15}H_{16}N_2O_2$: C, 70.29; H, 6.29; N, 10.93. Found: C, 70.19; H, 6.17; N, 11.02.

*4.3.6. 1-[(1-Hydroxy-2-naphthylmethylen)amino]-4-methylpiperazine (**23**).* From 1-hydroxy-2-naphthaldehyde and 1-amino-4-methylpiperazine (51%); mp 122–123 °C, IR ($\nu$, KBr): 1629 (CH=N), 1586, 1561, 1507, 1451 $cm^{-1}$ (arom). $^1H$ NMR (400 MHz, $CDCl_3$): $\delta$ 12.73 (1H, s, OH), 8.38 (1H, m, H-arom), 7.84 (1H, s, CH=N), 7.77 (1H, m, H-arom), 7.50 (2H, m, H-arom), 7.35 (1H, d, $J$=8.4 Hz, H-arom), 7.25 (1H, d, $J$=8.4 Hz, H-arom), 3.26 (4H, t, $J$=4.8 Hz, $CH_2$), 2.68 (4H, t, $J$=5.0 Hz, $CH_2$), 2.40 (3H, s, $CH_3$). $^{13}C$ NMR (100 MHz, $CDCl_3$): $\delta$ 154.5 (C–OH), 141.5 (CH=N), 134.1, 127.4, 127.1, 126.4, 125.3, 125.0, 122.8, 118.5, 112.0 (C-arom), 54.2 ($CH_2$), 51.3 ($CH_2$), 45.9 ($CH_3$). Anal. Calcd for $C_{16}H_{19}N_3O$: C, 71.35; H, 7.11; N, 15.60. Found: C, 71.49; H, 7.25; N, 15.50.

*4.3.7. 1-[(1-Hydroxy-2-naphthylmethylen)amino]piperidine (**24**).* From 1-hydroxy-2-naphthaldehyde and 1-aminopiperidine (25%); mp 55–56 °C, IR ($\nu$, KBr): 1632 (CH=N), 1579, 1558, 1503, 1461 $cm^{-1}$ (arom). $^1H$ NMR (400 MHz, $CDCl_3$): $\delta$ 12.95 (1H, s, OH), 8.39 (1H, m, H-arom), 7.83 (1H, s, CH=N), 7.78 (1H, m, H-arom), 7.51 (2H, m, H-arom), 7.35 (1H, d, $J$=8.4 Hz, H-arom), 7.25 (1H, d, $J$=8.4 Hz, H-arom), 3.19 (4H, t, $J$=5.6 Hz, $CH_2$), 1.82 (4H, m, $CH_2$), 1.59 (2H, m, $CH_2$). $^{13}C$ NMR (100 MHz, $CDCl_3$): $\delta$ 154.4 (C–OH), 140.3 (CH=N), 133.9, 127.4, 126.9, 126.3, 125.2, 125.1, 122.8, 118.4, 112.4 (C-arom), 52.4 ($CH_2$), 24.9 ($CH_2$), 23.9 ($CH_2$). Anal. Calcd for $C_{16}H_{18}N_2O$: C, 75.56; H, 7.13; N, 11.01. Found: C, 75.39; H, 7.07; N, 10.85.

*4.3.8. 2,6-Dimethyl-1-[(1-hydroxy-2-naphthylmethylen)amino]piperidine (**25**).* From 1-hydroxy-2-naphthaldehyde and 1-amino-2,6-dimethylpiperidine (24%); mp 89–90 °C, IR ($\nu$, KBr): 1629 (CH=N), 1604, 1568, 1543, 1505 $cm^{-1}$ (arom). $^1H$ NMR (400 MHz, $CDCl_3$): $\delta$ 13.43 (1H, s, OH), 8.40 (1H, d, $J$=8.4 Hz, H-arom), 8.37 (1H, s, CH=N), 7.72 (1H, d, $J$=7.2 Hz, H-arom), 7.50 (2H, m, H-arom), 7.22 (2H, s, H-arom), 2.85 (2H, s, CH), 1.77 (3H, s, $CH_2$), 1.49 (3H, m, $CH_2$), 1.03 (6H, d, $J$=6.4 Hz, $CH_3$). $^{13}C$ NMR (100 MHz, $CDCl_3$): $\delta$ 163.0 (C–OH), 162.8 (CH=N), 135.8, 128.6, 127.4, 127.3, 126.2, 125.3, 123.8, 117.6, 109.5 (C-arom), 60.0 (CH), 33.2 ($CH_2$), 23.3 ($CH_2$), 21.2 ($CH_3$). Anal. Calcd for $C_{18}H_{22}N_2O$: C, 76.56; H, 7.85; N, 9.92. Found: C, 76.51; H, 7.74; N, 9.74.

## Acknowledgements

This work was supported by the Junta de Extremadura (PRI08A032) and the Ministerio de Educación y Ciencia and FEDER (CTQ2010-18938 and CTQ2007-66641). One of us (R.F.M.) thanks the Junta de Extremadura for a fellowship. We gratefully thank the Research & Technological Innovation and Supercomputing Center of Extremadura (CénitS) for allowing us the use of LUSITANIA computer resources. We also thank the referee for a series of valuable suggestions to improve the level of calculations.

## Supplementary data

Tables 1S and 2S, copies of NMR spectra and Cartesian coordinates of compounds **20**, **21**, **26**, **27**, and transition states. Supplementary data associated with this article can be found in online version at doi:10.1016/j.tet.2011.01.065.

## References and notes

1. Ogawa, K.; Harada, J. *J. Mol. Struct.* **2003**, *647*, 211–216.
2. Dominiak, P.; Grech, E.; Barr, G.; Teat, S.; Mallinson, P. R.; Wozniak, K. *Chem. —Eur. J.* **2003**, *9*, 963–970.
3. (a) Hadjoudis, E. In *Studies in Organic Chemistry*; Durr, H., Bouas-Laurent, H., Eds.; Elsevier: Amsterdam, 1990; Vol. 40, Chapter 17; (b) Hadjoudis, E. *Mol. Eng.* **1995**, *5*, 301–307.
4. Feringa, B. L.; Jager, W. F.; Lange, B. *Tetrahedron* **1993**, *49*, 8267–8310.
5. Petkov, I. In *Organic Nanophotonics*; Science Series, N. A. T. O., Charra, F., Agramovich, V. M., Kajzar, F., Eds.; Kluwer: Dordrecht, 2002; pp 57–72.
6. For a review about the structure of hydrazones, see: Kitaev, Y. P.; Buzykin, B. I.; Troepol'skaya, T. V. *Russ. Chem. Rev.* **1970**, *39*, 441–456.
7. Sthephen, M.; van Schalkwyk, T. G. D.; Ravenscroft, N. *Arkivoc* **2002**, *3*, 103–111.
8. (a) Jain, M. P.; Kumar, S. *Talanta* **1977**, *24*, 149–150; (b) Okafor, E. C. *Talanta* **1978**, *25*, 241–242.
9. (a) Monfared, H. H.; Pouralimardan, O.; Janiak, C. *Z. Naturforsch.* **2007**, *62b*, 717–720; (b) Jing, Z.-L.; Yu, M.; Chen, X.; Diao, C.-H.; Deng, Q.-L.; Fan, Z. *Acta Crystallogr.* **2005**, *E61*, 145–146.
10. (a) Alyar, S.; Özmen, ÜÖ; Karacan, N.; Şentürk, O. Ş; Udachin, K. A. *J. Mol. Struct.* **2008**, *889*, 144–149; (b) Ali, H. M.; Laila, M.; Wan Jefrey, B.; Ng, S. W. *Acta Crystallogr.* **2007**, *E63*, 1617–1618; (c) Ali, H. M.; Laila, M.; Wan Jefrey, B.; Ng, S. W. *Acta Crystallogr.* **2007**, *E63*, 1619–1620; (d) Ali, H. M.; Laila, M.; Wan Jefrey, B.; Ng, S. W. *Acta Crystallogr.* **2007**, *E63*, 1821–1822; (e) Laila, M.; Ali, H. M.; Puvaneswary, S.; Robinson, W. T.; Ng, S. W. *Acta Crystallogr.* **2008**, *E64*, 1769–1770; (f) Lyubchova, A.; Cossé-Barbi, A.; Doucet, J. P.; Robert, F.; Souron, J.-P.; Quarton, M. *Acta Crystallogr.* **1995**, *C51*, 1893–1895.
11. Abboud, K. A.; Summers, S. P.; Palenik, G. J. *Acta Crystallogr.* **1995**, *C51*, 1707–1709.
12. (a) Novak, P.; Pičuljan, K.; Hrenar, T.; Biljan, T.; Meić, Z. *J. Mol. Struct.* **2008**, *919*, 66–71; (b) Swesi, A. T.; Farina, Y.; Kassim, M.; Ng, S. W. *Acta Crystallogr.* **2006**, *E62*, 5457–5458; (c) Koo, C. H.; Kim, H. S.; Ahn, C. T. *J. Korean Chem. Soc.* **1977**, *21*, 3–15.
13. Hökelek, T.; Bilge, S.; Kiliç, Z. *Anal. Sci.* **2006**, *22*, 115.
14. Sluis-Cremer, N.; Arion, D.; Parniak, M. A. *Mol. Pharmacol.* **2002**, *62*, 398–405.
15. Ivannou, P. C.; Konstantianos, D. G. *Clin. Chem.* **1989**, *35*, 1492–1496.
16. Richardson, D. R.; Bernhardt, P. V. *J. Biol. Inorg. Chem.* **1999**, *4*, 266–273.
17. (a) Tsaplev, Y. B. *High Energy Chem.* **2005**, *39*, 100–105; (b) Vasil'ev, R. F.; Tsaplev, Y. B. *Russ. Chem. Rev.* **2006**, *75*, 989–1002.
18. Wu, Z.-H.; Ma, J.-P.; Wu, X.-W.; Huang, R.-Q.; Dong, Y.-B. *Acta Crystallogr.* **2009**, *C65*, 128–130.
19. Tai, X.-S.; Xu, J.; Feng, Y.-M.; Liang, Z.-P. *Acta Crystallogr.* **2008**, *E64*, 904–905.
20. Jesaitis, R. G. *Theor. Chim. Acta* **1973**, *32*, 71–75.
21. (a) Smith, M. B.; March, J. *Advanced Organic Chemistry*, 5th ed.; John Wiley: New York, NY, 2001; p 445; (b) Klopman, G.; Tsuda, K.; Louis, J. B.; Davis, R. E. *Tetrahedron* **1970**, *26*, 4549–4554.
22. Yildiz, M.; Ünver, H.; Dülger, B.; Erdener, D.; Ocak, N.; Erdönmez, A.; Durlu, T. N. *J. Mol. Struct.* **2005**, *738*, 253–260.
23. (a) Nakanishi, K.; Solomon, P. H. *Infrared Absorption Spectroscopy*, 2nd ed.; Holden-Day: San Francisco, 1977; p 34; (b) Nakanishi, K.; Solomon, P. H. *Infrared Absorption Spectroscopy*, 2nd ed.; Holden-Day: San Francisco, 1977; p 38.
24. X-ray diffraction analysis of compound **18** has been previously determined (Ref. 22) at 293 K. It has now been determined at 120 K. Crystal data for compounds **18**, **20**, **23** have been deposited with the Cambridge Crystallographic Data Centre (CCDC-794461, CCDC-794462, and CCDC-794460) and can

be obtained, upon request, from the Director, Cambridge Crystallographic Data Centre, 12 Union Road, Cambridge CB2 1EZ, UK.
25. (a) Becke, A. D. *J. Chem. Phys.* **1993**, *98*, 5648–5652; (b) Lee, C.; Yang, W.; Parr, R. G. *Phys. Rev. B* **1988**, *37*, 785–789.
26. Frisch, M. J.; Trucks, G. W.; Schlegel, H. B.; Scuseria, G. E.; Robb, M. A.; Cheeseman, J. R.; Scalmani, G.; Barone, V.; Mennucci, B.; Petersson, G. A.; Nakatsuji, H.; Caricato, M.; Li, X.; Hratchian, H. P.; Izmaylov, A. F.; Bloino, J.; Zheng, G.; Sonnenberg, J. L.; Hada, M.; Ehara, M.; Toyota, K.; Fukuda, R.; Hasegawa, J.; Ishida, M.; Nakajima, T.; Honda, Y.; Kitao, O.; Nakai, H.; Vreven, T.; Montgomery, J. A., Jr.; Peralta, J. E.; Ogliaro, F.; Bearpark, M.; Heyd, J. J.; Brothers, E.; Kudin, K. N.; Staroverov, V. N.; Kobayashi, R.; Normand, J.; Raghavachari, K.; Rendell, A.; Burant, J. C.; Iyengar, S. S.; Tomasi, J.; Cossi, M.; Rega, N.; Millam, N. J.; Klene, M.; Knox, J. E.; Cross, J. B.; Bakken, V.; Adamo, C.; Jaramillo, J.; Gomperts, R.; Stratmann, R. E.; Yazyev, O.; Austin, A. J.; Cammi, R.; Pomelli, C.; Ochterski, J. W.; Martin, R. L.; Morokuma, K.; Zakrzewski, V. G.; Voth, G. A.; Salvador, P.; Dannenberg, J. J.; Dapprich, S.; Daniels, A. D.; Farkas, Ö; Foresman, J. B.; Ortiz, J. V.; Cioslowski, J.; Fox, D. J. *Gaussian 09, Revision B.01*; Gaussian: Wallingford CT, 2009.
27. (a) Zhao, Y.; Truhlar, D. G. *Acc. Chem. Res.* **2008**, *41*, 157–167; (b) Zhao, Y.; Truhlar, D. G. *Theor. Chem. Acc.* **2008**, *120*, 215–241.
28. Marenich, A. V.; Cramer, C. J.; Truhlar, D. G. *J. Phys. Chem. B* **2009**, *113*, 6378–6396.
29. (a) Eliel, E. L.; Allinger, N. L.; Angyal, S. J.; Morrison, G. A. *Conformational Analysis*; Wiley: New York, NY, 1965; p 245; (b) Allinger, N. L.; Carpenter, J. G. D.; Karkowski, F. M. *Tetrahedron Lett.* **1964**, *5*, 3345–3349; (c) Eliel, E. L.; Wilen, S. H. *Stereochemistry of Organic Compounds*; Wiley: New York, NY, 1994; p 741.
30. The chair conformational reversal barrier for *N*-methylpiperidine is 11.9 kcal $mol^{-1}$; see Ref. 29c.
31. Reed, A. E.; Curtiss, L. A.; Weinhold, F. *Chem. Rev.* **1988**, *88*, 899–926.
32. Hooft, R.; Nonius, B. V. *COLLECT: Data Collection Software*; Nonius BV: The Netherlands, 1998.
33. Otwinowski, Z.; Minor, W. Processing of X-ray diffraction data collected in oscillation mode In *Macromolecular Crystallography, Part A*; CarterJr., C. W., Sweet, R. M., Eds.; Methods in Enzymology; Academic: San Diego, CA, 1997; Vol. 276, pp 307–326.
34. Sheldrick, G. M. SADABS–Bruker Nonius Area Detector Scaling and Absorption Correction-v2.10, 1993.
35. Sheldrick, G. M. *SHELX97: Programs for Crystal Structure Analysis (Release 97–2)*; Institüt für Anorganische Chemie der Universität, Tammanstrasse 4, D-3400: Göttingen, Germany, 1998.
36. Watkin, D. M.; Pearce, L.; Prout, C. K. *CAMERON. A Molecular Graphics Package*; Chemical Crystallography Laboratory, University of Oxford: England, 1993.